CHEMISTRY
AN ASIAN JOURNAL
www.chemasianj.org

Accepted Article

Title: Achieving Purely-Organic Room-Temperature Aqueous Phosphorescence via Two-Component Macromolecular Self-Assembly Strategy

Authors: Wang Guo, Xuepu Wang, Bei Zhou, and Kaka Zhang

To be cited as: *Chem. Asian J.* 10.1002/asia.202000965

Link to VoR: https://doi.org/10.1002/asia.202000965

A Journal of
ACES Asian Chemical Editorial Society

A sister journal of Angewandte Chemie and Chemistry – A European Journal

WILEY-VCH

10.1002/asia.202000965

WILEY-VCH

Achieving Purely-Organic Room-Temperature Aqueous Phosphorescence via Two-Component Macromolecular Self-Assembly Strategy

Wang Guo, Xuepu Wang, Bei Zhou and Kaka Zhang*

[a] Key Laboratory of Synthetic and Self-Assembly Chemistry for Organic Functional Molecules,
Shanghai Institute of Organic Chemistry, University of Chinese Academy of Sciences, Chinese Academy of Sciences,
345 Lingling Road, Shanghai 200032, People's Republic of China
E-mail: zhangkaka@sioc.ac.cn

Supporting information for this article is given via a link at the end of the document.((Please delete this text if not appropriate))

Abstract: Manipulation of supramolecular behaviors and aggregation states represent an important topic in devising intriguing photofunctional systems. Here we report a two-component macromolecular self-assembly strategy for achieving aqueous room-temperature phosphorescence (RTP) in purely organic systems. Amphiphilic triblock copolymers are used to modulate the self-assembly of planar RTP molecules in aqueous solution, leading to the formation of sheet-like RTP objects with well-defined morphology, uniform crystalline nanostructures and excellent aqueous dispersity. In contrast, the addition of the planar RTP molecules into aqueous medium only leads to precipitation and quenching of RTP properties. Powder X-ray diffraction and single crystal X-ray diffraction studies reveal that the amphiphilic triblock copolymers can assist supramolecular columnar packing of the planar RTP molecules where multiple non-covalent interactions stabilize the triplet excited states. Interestingly, it is found that luminescent signals of the sheet-like RTP objects can be extracted from strong fluorescent environments by phosphorescence mode and emission lifetime measurement.

Introduction

The manipulation of supramolecular behaviors and aggregation states plays an important role for the fabrication of luminescent materials with intriguing photophysical properties.[1,2] Block copolymers have been reported by us and others to modulate the supramolecular behaviors of small molecules in macromolecular self-assembly systems where the polymers can noncovalently interact with the small molecules.[3-9] This two-component design strategy allows a flexible choice of building blocks with less synthetic effort.

Recent studies show that room-temperature phosphorescence (RTP) in purely organic systems has emerged as an important topic in the field of luminescent materials.[10-15] Characteristic of their long-lived excited states, organic RTP materials show superior performance in oxygen sensing,[16,17] advanced anti-counterfeiting[14,18,19] and high-contrast bioimaging,[20-26] when compared to conventional organic fluorescent materials. Due to the intrinsically spin-forbidden nature of the phosphorescent emission, the RTP properties in purely organic systems can be easily quenched by nonradiative deactivation processes. The aggregation states of the organic RTP molecules have a large influence on their phosphorescence properties. Most of the reported RTP phenomena in purely organic systems can only be observed in molecular crystalline states where the nonradiative deactivation of the triplet excited states can be effectively suppressed.[10-35] However, the molecular crystals usually lack solution dispersity,[10-39] which limits the applications of these RTP materials.

Nanoprecipitation has been reported to endow these RTP materials with aqueous dispersity.[14] RTP dispersion in aqueous medium can be obtained by injection of the RTP solution into water, whereas the RTP dispersion can undergo further aggregation to form macroscopic precipitates upon long-term storage due to the hydrophobic nature of the RTP molecules, as well as the absence of steric or electrostatic repulsion effects for particle dispersion. With the aid of surfactant and sonication,[20,22] well-dispersed spherical RTP nanoparticles have been obtained by bottom-up pathways, while anisotropic nanostructures with well-defined crystalline structures that can maintain RTP properties have been rarely reported. A recent study shows that the bottom-up pathway may cause the loss of RTP performance in the resultant products.[22] Therefore, it remains a challenging task to fabricate RTP nanostructures with excellent aqueous dispersity and well-defined crystalline structures where the nonradiative deactivation of the triplet excited states can be largely inhibited.

In the present study, based on molecular design and extensive screening, an efficient RTP system of 9-acetyl-3,6-diiodocarbazole in the crystalline solid state has been found to exhibit highly efficient intersystem crossing and pure phosphorescence (fluorescence free) in its steady-state emission spectra. The addition of the planar RTP molecules into aqueous medium has been found to only lead to the precipitation and quenching of RTP properties. In striking contrast, sheet-like crystalline nanostructures that show well-defined morphology, excellent aqueous dispersity and maintain RTP properties have been fabricated through the macromolecular self-assembly of 9-acetyl-3,6-diiodocarbazole and an amphiphilic triblock copolymer. It has been also found that, in a strong fluorescent environment, the luminescent signals of the sheet-like crystalline nanostructures can be extracted by phosphorescence mode and emission lifetime measurements, exhibiting characteristics for promising phosphorescence and lifetime imaging applications.

Results and Discussion

9-Acetyl-3,6-diiodocarbazole (RTP-8) was prepared by a three-step reaction from diphenylamine according to the procedures as shown in Scheme 1A. RTP-8 was purified by column chromatography followed by recrystallization in dichloromethane/methanol for three times to give white solids. Colorless needle-like single crystals can be grown from dichloromethane/hexane. ^{1}H NMR, ^{13}C{^{1}H} NMR, LRMS, HRMS, FT-IR, melting point measurement, elemental analysis and single crystal X-ray diffraction of RTP-8 all give satisfactory results (Figure S1-S6), which reveal its structure and high purity.

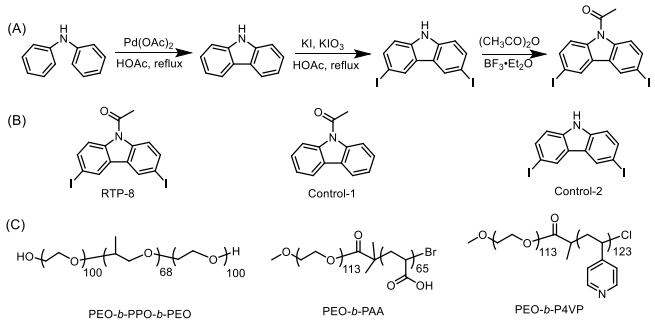

Scheme 1. (A) Synthesis of 9-acetyl-3,6-diiodocarbazole from diphenylamine. (B) Structure of RTP-8 and control samples. (C) Structure of block copolymers.

At room temperature, RTP-8 solid samples emit bright yellow light under a 365 nm UV lamp (Figure 1A). With the aid of UV curable resin and silicone molds (Experimental Section), RTP-8 powders can be readily processed into objects with arbitrary shapes and tailorable sizes (Figure 1B). Figure 1C displays SIOC-shaped RTP-8/resin composites which emit bright yellow light upon 365 nm irradiation. The steady-state emission spectra of RTP-8 solids exhibit a structured emission band with three peaks at 497, 539 and 578 nm (Figure 2A). Emission lifetimes (Figure 2B) fit to double-exponential decay (τ_1 = 0.1 ms, τ_2 = 1.6 ms) probably due to heterogeneous microenvironments in the RTP-8 powders where domains with different crystallinities coexist.[10]

Figure 1. Digital photographs of (A) RTP-8 solids under 365 nm UV lamp, (B) SIOC-shaped RTP-8/resin composites under ambient light and (C) SIOC-shaped RTP-8/resin composites under 365 nm UV lamp.

Organic RTP materials dispersed in aqueous solution, especially in physiological conditions, is essential for their potential application in diverse areas. To endow the RTP materials with aqueous dispersity, nanoprecipitation method was first tested. The addition of 0.2 mL of RTP-8 solution in THF (3 mg/mL) to 1.8 mL deionized water only leads to the macroscopic precipitation of RTP-8 solids (Figure S7) with low crystallinity (PXRD pattern shown in Figure 3). The RTP-8 precipitates with low crystallinity show the absence of yellow emission under 365 nm UV lamp (Figure S7). When compared to the bright yellow emission of RTP-8 crystalline solids with relatively high crystallinity (Figure 1A), these observations suggest that the luminescent properties of RTP-8 samples are strongly related to their aggregation states, that is, sample crystallinity.

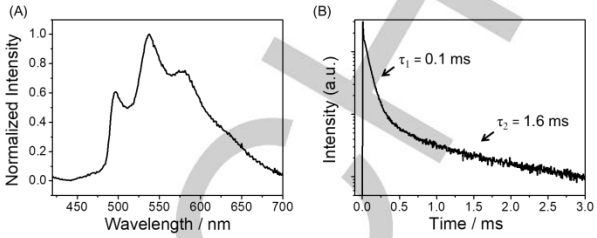

Figure 2. (A) Room-temperature steady-state emission spectra of RTP-8 crystalline solids (λ_{exi} = 400 nm). (B) Room-temperature emission decay profile at 539 nm of RTP-8 crystalline solids excited at 400 nm.

Macromolecular self-assembly of RTP-8 and amphiphilic triblock copolymers has also been performed in aqueous solution to fabricate RTP-8 nanostructures. Upon mixing RTP-8 (0.3 mg/mL) with Pluronic F-127 (2.7 mg/mL, PEO_{100}-*b*-PPO_{68}-*b*-PEO_{100}, the subscript represents the degree of polymerization of each block) in a mixed solvent of tetrahydrofuran-water (1:9, v/v), the clear aqueous solution first turns bluish and then becomes milky after incubation at room temperature for 10 minutes. RTP-8 nanostructures were collected by centrifugation after room-temperature incubation for 1 day and then redispersed in deionized water.

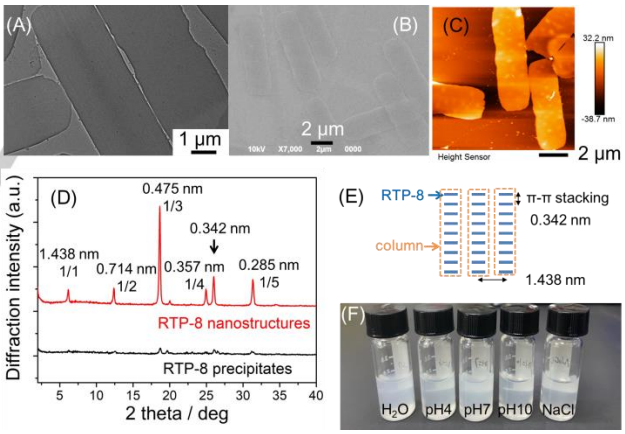

Figure 3. (A) TEM, (B) SEM and (C) AFM images of the sheet-like RTP-8 nanostructures. (D) PXRD pattern of RTP-8 nanostructures and RTP-8 precipitates. (E) Proposed packing of RTP-8 planar molecules within the crystalline nanostructure (top view). (F) RTP-8 nanostructures dispersed in deionized water, pH 4 water, pH 7 Tris-HCl buffer, pH 10 water and 150 mM NaCl aqueous solution.

TEM and SEM studies exhibit sheet-like RTP-8 nanostructures with well-defined morphologies (Figure 3A and 3B). The nanosheets possess a width of 2.2±0.2 μm and a length of 7.3±0.5 μm. AFM measurement shows that the nanosheets have a thickness of 30 nm (Figure 3C and Figure S8). The similar morphologies observed by different methods and the overlap between the nanosheets as shown in Figure 3B demonstrate that the nanosheets were formed in the solutions. Selected area electron diffraction studies that can be used to

investigate the molecular orientation within the RTP nanostructures gave no signals because of their instability in the electron beam. The powder X-ray diffraction (PXRD) pattern of a dried film of RTP-8 nanostructures exhibit a series of Bragg peaks with *d*-spacing following the ratios of 1 : 1/2 : 1/3 : 1/4 : 1/5 (Figure 3D). The appearance of higher order diffraction peaks is evidence of the high quality of crystalline growth of the sheet-like nanostructures. The diffraction peak at 2θ = 26.0° (*d* = 0.342 nm) shows the π–π stacking of RTP-8 planar molecules in the nanostructures. It is proposed that, during the macromolecular self-assembly, RTP-8 planar molecules stack into supramolecular columns by non-covalent π–π interactions and simultaneously the supramolecular columns undergo side-to-side packing in the lateral direction, leading to the formation of sheet-like crystalline nanostructures (Figure 3E). These observations indicate the important role of the Pluronic F-127 amphiphilic triblock copolymers in assisting the regular packing of planar RTP-8 molecules, when compared to the case of RTP-8 precipitates. It is noteworthy that crystalline nanostructures with such a well-defined morphology and regular molecular packing in the present study (Figure 3A-3C) have been rarely reported in purely organic RTP systems.[10-35] Other block copolymers (Scheme 1C) have also been used to assemble with RTP-8 in aqueous solutions. In the case of poly(ethylene oxide)-*b*-poly(acrylic acid) (PEO_{113}-*b*-PAA_{65}, the subscript represents the degree of polymerization of each block), macroscopic precipitates of RTP-8 formed (Figure S9). PEO_{113}-*b*-PAA_{65} block copolymers are double hydrophilic and cannot stabilize the neutral hydrophobic RTP-8 molecules. Poly(ethylene oxide)-*b*-poly(4-vinylpyridine) (PEO_{113}-*b*-$P4VP_{123}$) block copolymers are found to stabilize the hydrophobic RTP-8 molecules, whereas no yellow emission was observed in the resultant RTP-8/PEO_{113}-*b*-$P4VP_{123}$ aqueous suspension under 365 nm UV lamp (Figure S10).

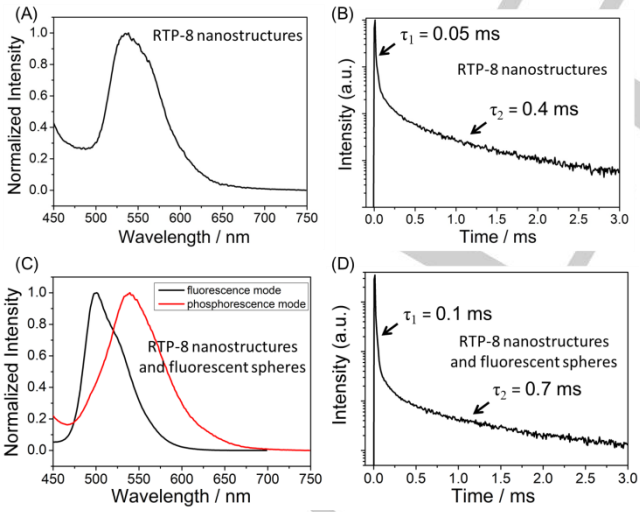

Figure 4. (A) Room-temperature steady-state emission spectra of RTP-8 nanostructures (λ_{exi} = 405 nm). (B) Room-temperature emission decay profile of RTP-8 nanostructures. (C) Room-temperature steady-state emission spectra (black spectrum, fluorescence mode; red spectrum, phosphorescence mode, chopping speed 40 Hz) of the mixture of RTP-8 nanostructures and fluorescent spheres (λ_{exi} = 405 nm). (D) Room-temperature emission decay profile of the mixture of RTP-8 nanostructures and fluorescent spheres.

RTP-8 nanostructures formed by the assistance of Pluronic F-127 are found to show excellent aqueous dispersity in acidic, neutral and basic conditions, as well as in 150 mM NaCl solution (Figure 3F), which can be attributed to the steric repulsion effect of PEO polymer chains of Pluronic F-127 for particle dispersion. The RTP-8 nanostructures have also been found to maintain excellent aqueous dispersity after storage in the ambient condition for weeks. Upon excitation at 405 nm, the steady-state emission spectra of RTP-8 nanostructures prepared from the assembly of RTP-8 and Pluronic F-127 exhibit emission band at 538 nm (Figure 4A). Emission lifetimes (Figure 4B) fit to double-exponential decay (τ_1 = 0.05 ms, τ_2 = 0.4 ms). When compared to RTP-8 precipitates (Figure S7), the emission band of RTP-8 nanostructures in the yellow region indicates that the photophysical properties of the RTP systems are strongly related to the aggregation states of the RTP molecules; emission intensity increases with sample crystallinity.

The luminescent properties of the RTP-8 nanostructures have also been tested in strong fluorescent environments. Upon the mixing of RTP-8 nanostructures and fluorescent spheres (carboxylate-modified polystyrene latex beads, 2.0 μm mean particle size, λ_{emi} ~ 505 nm, fluorescent yellow-green), the steady-state emission spectra of the mixture measured in the fluorescence mode are found to be dominated by the fluorescent spheres (Figure 4C). Interestingly, in the phosphorescence mode (Figure 4C), the emission spectra of the mixture recorded by a Hitachi FL-7000 spectrometer at chopping speed of 40 Hz are found to be very similar to those of the RTP-8 nanostructures (Figure 4A). Moreover, room-temperature emission decay profile of the mixture of RTP-8 nanostructures and fluorescent spheres exhibit double-exponential decay behaviors in the time region of several milliseconds, which is similar to that of the RTP-8 nanostructures (Figure 4B and 4D). These observations indicate that, because of their long-lived excited states, the aqueous dispersable RTP-8 nanostructures show the capability of removing the background fluorescent interference by phosphorescence mode and emission lifetime measurements.

To get further insight into the phosphorescence properties of the RTP-8 nanostructures, more photophysical studies of the RTP-8 crystalline solids have been performed. Figure 2A shows the structured emission band with three peaks at 497, 539 and 578 nm in the steady-state emission spectra of RTP-8 solids. It is found that the shape of the emission band and the peak wavelength show insignificant change upon the variation of the excitation wavelength (Figure S11), which suggests that the emission band in the range of 460 to 700 nm are originated from the same excited state. The excitation spectrum of RTP-8 solids shows a peak at 340 nm (Figure S12), similar to the UV-vis absorption spectrum of RTP-8 in thin film state (Figure S13). The large Stokes shift from 340 nm to 539 nm (10859 cm^{-1}) and the long-lived excited states (Figure 2B) confirm that RTP-8 represents an organic room-temperature phosphorescent material. Phosphorescence spectra of RTP-8 solids further confirm that the emission band in the range of 460 to 700 nm are originated from the triplet excited state of RTP-8 solids (Figure S14). The emission maximum of RTP-8 nanostructures is consistent with that of RTP-8 crystalline solids. The emission band of RTP-8 nanostructures (Figure 4A) is less structured than that of RTP-8 crystals (Figure 2A), which again suggest that the photophysical properties of RTP-8 are dependent on their aggregation states; the packing geometry of RTP-8 crystalline solids has been found to be different from that of

RTP-8 nanostructures (*vide infra*). The photoluminescent quantum efficiency of RTP-8 powders has been measured to be 4%. In control experiments, both 9-acetylcarbazole and 3,6-diiodocarbazole (Scheme 1B) don't show bright yellow emission under 365 nm UV lamp (Figure S15). These suggest the collaboration of heavy atom effect and n–π* transition in improving the phosphorescence efficiency in RTP-8 system. It is noteworthy that the reported carbazole RTP systems have been found to show fluorescence/phosphorescence dual emission behaviors.[27-32] A distinct feature of the present RTP system is the absence of fluorescence bands in its steady-state emission spectra, which indicates the highly efficient singlet-to-triplet intersystem crossing.

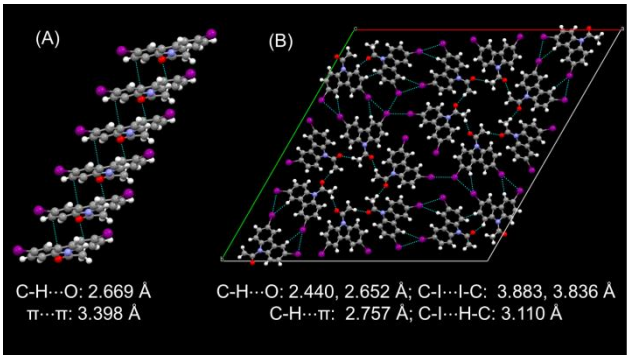

Figure 5. Single-crystal structures of RTP-8 showing (A) the head-to-head columnar stacking and (B) the multiple non-covalent interactions between neighboring RTP-8 supramolecular columns.

Single crystal X-ray diffraction studies reveal that planar RTP-8 molecules exhibit a head-to-head columnar stacking through π–π interactions (Figure 5A). The RTP-8 columns associate with neighbouring columns via multiple non-covalent interactions such as C–I···I–C halogen bonding, C–H···O interactions and others (Figure 5B). In the crystalline structures of RTP-8 nanostructures, the RTP-8 molecules retain supramolecular columnar stacking via π–π interactions (Figure 3D and 3E). Interestingly, the packing geometry of the supramolecular columns of RTP-8 nanostructures (Figure 3D and 3E) are different from that of RTP-8 single crystals (Figure 5B), which suggest that Pluronic F-127, as well as the solvent mixture used for macromolecular self-assembly, can influence and modulate the supramolecular and crystalline behaviors of the planar RTP-8 molecules. In the crystalline state where the microenvironment of RTP-8 is rigidified due to the presence of multiple non-covalent interactions, the nonradiative deactivation of triplet excited state can be suppressed in a large extent. Besides, the crystalline structure with close packed RTP-8 columns can protect the triplet excited state from oxygen quenching in the ambient condition. Further experiments show that the luminescent properties of the RTP-8 crystalline solids at ambient and in vacuum possess insignificant difference (Figure S16). It is also found that the steady-state emission spectra exhibit insignificant change when the RTP-8 crystalline solids are exposed to different aqueous environments (Figure S17).

Conclusion

All the above photophysical studies and structural analysis indicate the importance of the two-component design strategy for achieving purely-organic room-temperature aqueous phosphorescence. The amphiphilic triblock copolymers not only provide excellent aqueous dispersity but also assist the regular packing of planar RTP molecules into crystalline RTP nanostructures. In contrast, the addition of the RTP-8 molecules into aqueous medium only leads to the precipitation and quenching of RTP properties. The efficient RTP properties of the 9-acetyl-3,6-diiodocarbazole systems are associated with the introduction of heavy atom effect and n–π* transition, as well as the formation of supramolecular columnar packing of carbazole molecules where multiple non-covalent interactions in the crystalline nanostructures stabilize the triplet excited states. Taking advantage of their relatively long-lived excited state when compared to fluorescent systems, the aqueous dispersable RTP-8 nanostructures exhibit the capability of removing the background fluorescent interference and show characteristics for promising phosphorescence imaging and emission lifetime imaging applications. Further study will also be placed on the fabrication of purely organic aqueous RTP systems with higher photoluminescence quantum yields and longer luminescent lifetimes.

Experimental Section

Physical measurements and instrumentation

^{1}H NMR (400 MHz) and ^{13}C{^{1}H} NMR (100 MHz) spectra were recorded on a JEOL Fourier-transform NMR spectrometer (400 MHz) with chemical shifts reported relative to tetramethylsilane. Mass spectra were performed on Agilent Technologies 5973N and Thermo Fisher Scientific LTQ FT Ultras mass spectrometer. FT-IR spectra were recorded on a Nicolet AVATAR-360 FT-IR spectrophotomerter with a resolution of 4 cm^{-1}. Differential scanning calorimetry (DSC) was performed on a TA Q200 DSC instrument in nitrogen with a heating rate of 20 °C/min. Elemental analysis was carried out on a Carlo-Erba1106 system. UV-Vis absorption spectra were recorded on a Hitachi U-3310 UV-vis spectrophotometer. Emission spectra were recorded using Edinburgh FLS1000 fluorescence spectrometer, Hitachi FL-7000 and FL-2700 fluorescence spectrometer. The phosphorescence spectra were collected by a Hitachi FL-7000 fluorescence spectrometer. During the measurements, chopping speed was fixed at 40 Hz and the PMT voltage is fixed at 700 V. Photoluminescence quantum yield was measured by a Hamamatsu absolute PL quantum yield measurement system. Transmission electron microscopy (TEM) experiments were performed on a JEOL JEM-1230 transmission electron microscope with an accelerating voltage of 80 kV. Scanning electron microscopy (SEM) experiments were carried out on a JSM-6390LV scanning electron microscope. Step-scanned powder X-ray diffraction (PXRD) data were collected on a PANalytical X'Pert powder system using monochromated Cu/Kα (λ = 0.154 nm).

Synthesis of 9-acetyl-3,6-diiodocarbazole

9-Acetyl-3,6-diiodocarbazole (RTP-8) was synthesized from diphenylamine by a three-step reaction. (Step 1) Diphenylamine (0.50 g, 2.95 mmol), palladium(II) acetate (0.26 g, 1.18 mmol) and 2.0 mL acetic acid were added to a round-bottle flask to react at 80 °C for 7 h.[40] Carbazole (0.30g, 60% yield) was purified by column chromatography (15:1, v/v, petroleum ether/ethyl acetate). (Step 2) Carbazole (0.25 g, 1.49 mmol), potassium iodide (0.32g, 1.93 mmol), potassium iodate (0.48 g, 2.24 mmol) and 2.0 mL acetic acid were added to a round-bottle flask to react at 80 °C for 2 h.[41] 3,6-Diiodo-9H-carbazole (0.50 g, 80% yield)

was purified by column chromatography (10:1, v/v, petroleum ether/ethyl acetate). (Step 3) 3,6-Diiodo-9H-carbazole (0.4 g, 0.95 mmol), acetic anhydride (2 mL) and boron trifluoride diethyl etherate (20 µL) were added to a round-bottle flask and refluxed at 80 °C for 1h.[41] 9-Acetyl-3,6-diiodocarbazole (0.36 g, 85% yield) was purified by column chromatography (10:1, v/v, petroleum ether/ethyl acetate). Recrystallization in dichloromethane/methanol for three times was applied for the further purification of the 9-acetyl-3,6-diiodocarbazole samples to give white solids. Melting point of 9-acetyl-3,6-diiodocarbazole was measured by DSC to be 228 °C. ^{1}H NMR (400 MHz, $CDCl_3$, 298 K, δ/ppm): δ = 2.83 (s, 3H), 7.75 (dd, J = 8.8, 1.8 Hz, 2H), 7.94 (d, J = 8.8 Hz, 2H), 8.23 (d, J = 1.8 Hz, 2H). ^{13}C{^{1}H} NMR (100 MHz, $CDCl_3$, 298 K, δ/ppm): δ = 27.7, 87.6, 118.0, 127.2, 129.0, 136.5, 138.0, 169.7. FT-IR (KBr, cm^{-1}): v 3060, 2998, 2924, 1737, 1706, 1670, 1607, 1574, 1468, 1424, 1393, 1379, 1345, 1304, 1278, 1209, 1067, 1058, 1044, 1025, 1015, 980, 868, 820, 811, 798. LRMS, m/z 461. HRMS m/z found (calcd for $C_{14}H_{10}ONI_2$): 461.8852 (461.8846). Elemental analysis calcd (%) for $C_{14}H_{10}ONI_2$: C 36.47, H 1.97, N 3.04; found: C 36.03, H 1.75, N 2.93.

Preparation of SIOC-shaped RTP-8/resin composites

RTP-8 powders were added to the liquid precursor of UV curable polyacrylate resin by stirring. The obtained suspension of RTP-8 powders in the liquid precursor was transferred to silicon molds. After irradiation under 365 nm UV light for 20 min, the SIOC-shaped RTP-8/resin composites were obtained.

Preparation of Pluronic F-127 aqueous solution

Pluronic F-127 (poly(ethylene oxide)-*b*-poly(propylene oxide)-*b*-poly(ethylene oxide), PEO_{100}-*b*-PPO_{68}-*b*-PEO_{100}, the subscript represents the degree of polymerization of each block, Sigma-Aldrich) was dissolved in deionized water at 3.0 mg/mL by magnetic stirring before use.

Synthesis of PEO-*b*-PAA block copolymers

The macroinitiator PEO_{113}-Br (the subscript represents the degrees of polymerization) was first synthesized according to the literature methods, [42] and then the poly(ethylene oxide)-*b*-poly(*tert*-butyl acrylate) (PEO-*b*-P*t*BA) diblock copolymers were synthesized via atom transfer radical polymerization (ATRP).[43] For the polymerization of *tert*-butyl acrylate (*t*BA), the mixture of PEO_{113}-Br, CuBr and toluene, and the mixture of *N*,*N*,*N'*,*N''*,*N''*-pentamethyldiethylenetriamine (PMDETA) and *t*BA, were degassed respectively via nitrogen bubbling and then mixed together. The molar ratio of PEO_{113}-Br/CuBr/PMDETA in the reaction mixture was 1/0.5/0.5, and the degrees of polymerization of P*t*BA were controlled by *t*BA/PEO_{113}-Br feed ratio. The polymerization was conducted at 100 °C in an oil bath and finally quenched in an ice bath. The copper complex in the reaction mixture was removed by passing the reaction mixture through neutral Al_2O_3 column using dichloromethane as an eluent. PEO_{113}-*b*-P*t*BA_{65} block copolymers (M_w/M_n = 1.20) were obtained. The degrees of polymerization of the P*t*BA blocks and M_w/M_n of the PEO_{113}-*b*-P*t*BA_{65} block copolymers were determined by ^{1}H NMR and gel permeation chromatography (GPC), respectively. To prepare poly(ethylene oxide)-*b*-poly(acrylic acid) (PEO-*b*-PAA), PEG_{113}-*b*-P*t*BA_{65} block copolymers were first dissolved in dichloromethane (DCM) at approximately 50 mg/mL, and then trifluoroacetic acid (TFA) was added at a TFA/DCM volume ratio of 1/10 to the solution to selectively hydrolyze the *tert*-butyl ester groups. After hydrolysis for 2 days, the reaction mixture was evaporated under reduced pressure to dryness. The PEO_{113}-*b*-PAA_{65} block copolymers obtained were purified by four cycles of dissolution in methanol/precipitation in hexane. The deprotection of the *tert*-butyl ester groups was confirmed by FTIR and ^{1}H NMR spectroscopy.

Synthesis of PEO-*b*-P4VP block copolymers

The macroinitiator PEO_{113}-Cl (the subscript represents the degrees of polymerization) was first synthesized according to the literature methods,[44] and then the poly(ethylene oxide)-*b*-poly(4-vinylpyridine) (PEO-*b*-P4VP) diblock copolymers were synthesized via ATRP.[45] For the polymerization of 4-vinylpyridine (4VP), the mixture of PEO_{113}-Cl, CuCl and isopropanol, and the mixture of tris[2-(dimethylamino)ethyl]amine (Me_6TREN) and 4VP, were degassed respectively via nitrogen bubbling and then mixed together. The molar ratio of PEO_{113}-Cl/CuCl/Me_6TREN in the reaction mixture was 1/0.5/0.5, and the degrees of polymerization of P4VP were controlled by 4VP/PEO_{113}-Cl feed ratio. The polymerization was conducted at 50 °C in an oil bath and finally quenched in an ice bath. The copper complex in the reaction mixture was removed by passing the reaction mixture through neutral Al_2O_3 column using dichloromethane as an eluent. PEO_{113}-*b*-$P4VP_{123}$ block copolymers (M_w/M_n = 1.25) were purified by three cycles of dissolution in dichloromethane/precipitation in diethyl ether. The degrees of polymerization of the P4VP blocks and M_w/M_n of the PEO_{113}-*b*-$P4VP_{123}$ block copolymers were determined by ^{1}H NMR and GPC, respectively.

Preparation of RTP-8 nanostructures

0.2 mL of RTP-8 solution in tetrahydrofuran (3.0 mg/mL) was mixed with 1.8 mL of Pluronic F-127 solution in deionized water (3.0 mg/mL). The mixture was homogenized by gentle shaking. The clear aqueous solution first turns bluish and then becomes milky after incubation at room temperature for 10 minutes. RTP-8 nanostructures were collected by centrifugation after room-temperature incubation for 1 day and then redispersed in deionized water.

Formation of strong fluorescent environments for RTP-8 nanostructures

Carboxylate-modified polystyrene latex beads (Sigma-Aldrich L4530, 2.5% aqueous suspension, 2.0 µm mean particle size, λ_{emi} ~505 nm, fluorescent yellow-green) were mixed with RTP-8 nanostructures at a sphere/RTP-8 mass ratio of approximately 1:1. The mixture shows bright yellow-green emission color under 365 nm UV lamp. Room-temperature steady-state emission measurements in both fluorescence and phosphorescence modes, as well as the emission decay properties of the mixture of fluorescent spheres and RTP-8 nanostructures were performed to investigate the photophysical properties of RTP-8 nanostructures in the strong fluorescent environments formed by the fluorescent spheres.

Acknowledgements ((optional))

We thank the financial supports from Shanghai Scientific and Technological Innovation Project (20QA1411600, 20ZR1469200), and Hundred Talents Program from Shanghai Institute of Organic Chemistry (Y121078). The National Facility for Protein Science (NFPS) of the Shanghai Synchrotron Radiation Facility (SSRF) is acknowledged for providing beamline time (BL17B beamline). We thank Prof. Vivian W.-W. Yam and Mr. Liangliang Yan for their help in single crystal X-ray diffraction study.

Keywords: aggregation • block copolymers • nanostructures • phosphorescence • self-assembly

[1] V. W.-W. Yam, V. K.-M. Au, S. Y.-L. Leung, *Chem. Rev.* **2015**, *115*, 7589.
[2] J. Mei, N. L.-C. Leung, R. T.-K. Kwok, J. W.-Y. Lam, B. Z. Tang, *Chem. Rev.* **2015**, *115*, 11718.
[3] D. Chen, M. Jiang, *Acc. Chem. Res.* **2005**, *38*,494.
(4) M. Guo, M. Jiang, *Soft Matter* **2009**, *5*, 495.

[5] K. Zhang, S. Y.-L. Yeung, S. Y.-L. Leung, V. W.-W. Yam, *Chem* **2017**, *2*, 825.
[6] A. F. Thünemann, S. Kubowicz, C. Burger, M. D. Watson, N. Tchebotareva K. Müllen, *J. Am. Chem. Soc.* **2003**, *125*, 352.
[7] K. Zhang, S. Y.-L. Yeung, S. Y.-L. Leung, V. W.-W. Yam, *Proc. Natl. Acad. Sci. USA*, **2017**, *114*, 11844.
[8] M. Huang, U. Schilde, M. Kumke, M. Antonietti, H. Cölfen, *J. Am. Chem. Soc.* **2010**, *132*, 3700.
[9] K. Zhang, S. Y.-L. Yeung, S. Y.-L. Leung, V. W.-W. Yam, *J. Am. Chem. Soc.* **2018**, *140*, 9594.
[10] G. Zhang, J. Chen, S. J. Payne, S. E. Kooi, J. N. Demas, C. L. Fraser, *J. Am. Chem. Soc.* **2007**, *129*, 8942.
[11] W. Z. Yuan, X. Y. Shen, H. Zhao, J. W. Y. Lam, L. Tang, P. Lu, C. Wang, Y. Liu, Z. Wang, Q. Zheng, J. Z. Sun, Y. Ma, B. Z. Tang, *J. Phys. Chem. C* **2010**, *114*, 6090.
[12] J. Wang, X. Gu, H. Ma, Q. Peng, X. Huang, X. Zheng, S. H.-P. Sung, G. Shan, J. W.-Y. Lam, Z. Shuai, B. Z. Tang, *Nat. Commun.* **2018**, *9*, 2963.
[13] O. Bolton, K. Lee, H. J. Kim, K. Y. Lin, J. Kim, *Nat. Chem.* **2011**, *3*, 205.
[14] Z. An, C. Zheng, Y. Tao, R. Chen, H. Shi, T. Chen, Z. Wang, H. Li, R. Deng, X. Liu, W. Huang, *Nat. Mater.* **2015**, *14*, 685.
[15] S. Hirata, K. Totani, J. Zhang, T. Yamashita, H. Kaji, S. R. Marder, T. Watanabe, C. Adachi, *Adv. Funct. Mater.* **2013**, *23*, 3386.
[16] G. Zhang, G. M. Palmer, M. W. Dewhirst, C. L. Fraser, *Nat. Mater.* **2009**, *8*, 747.
[17] Y. Yu, M. S. Kwon, J. Jung, Y. Zeng, M. Kim, K. Chung, J. Gierschner, J. H. Youk, S. M. Borisov, J. Kim, *Angew. Chem. Int. Ed.* **2017**, *56*, 16207.
[18] J. Zhao, Z. He, J. W. Y. Chan, Q. Peng, H. Ma, Z. Shuai, G. Bai, J. Hao, B. Z. Tang, *Chem* **2016**, *1*, 592.
[19] J. Wei, B. Liang, R. Duan, Z. Cheng, C. Li, T. Zhou, Y. Yi, Y. Wang, *Angew. Chem. Int. Ed.* **2016**, *55*, 15589.
[20] J. Jin, H. Jiang, Q. Yang, L. Tang, Y.; Tao, Y. Li, R. Chen, C. Zheng, Q. Fan, K. Y. Zhang, Q. Zhao, W. Huang, *Nat. Commun*. **2020**, *11*, 842.
[21] X. F. Wang, H. Xiao, P. Z. Chen, Q. Z. Yang, B. Chen, C. H. Tung, Y. Z. Chen, L. Z. Wu, *J. Am. Chem. Soc*. **2019**, *141*, 5045.
[22] X. Zhen, Y. Tao, Z. An, P. Chen, C. Xu, R. Chen, W. Huang, K. Pu, *Adv. Mater.* **2017**, *29*, 1606665.
[23] Z. He, H. Gao, S. Zhang, S. Zheng, Y. Wang, Z. Zhao, D. Ding, B. Yang, Y. Zhang, W. Z. Yuan, *Adv. Mater.* **2019**, *31*, 1807222.
[24] Y. You, K. Huang, X. Liu, X. Pan, J. Zhi, Q. He, H. Shi, Z. An, X. Ma, W. Huang, *Small* **2020**, *16*, 1906733.
[25] J. Yang, X. Zhen, B. Wang, X. Gao, Z. Ren, J. Wang, Y. Xie, J. Li, Q. Peng, K. Pu, Z. Li, *Nat. Commun.* **2018**, *9*, 840.
[26] H. Shi, L. Zou, K. Huang, H. Wang, C. Sun, S. Wang, H. Ma, Y. He, J. Wang, H. Yu, W. Yao, Z. An, Q. Zhao, W. Huang, *ACS Appl. Mater. Interfaces* **2019**, *11*, 18103.
[27] Y. Gong, G. Chen, Q. Peng, W. Z.; Yuan, J. Xie, S. Li, Y. Zhang, B. Z. Tang, *Adv. Mater.* **2015**, *27*, 6195.
[28] Z. Mao, Z. Yang, Y. Mu, Y. Zhang, Y. F. Wang, Z. Chi, C. C. Lo, S. Liu, A. Lien, J. Xu, *Angew. Chem. Int. Ed.* **2015**, *54*, 6270.
[29] S. Cai, H. Shi, J. Li, L. Gu, Y. Ni, Z. Cheng, S. Wang, W. W. Xiong, L. Li, Z. An, W. Huang, *Adv. Mater.* **2017**, *29*, 1701244.
[30] Y. Xie, Y. Ge, Q. Peng, C. Li, Q. Li, Z. Li, *Adv. Mater*. **2017**, *29*, 1606829.
[31] N. Gan, X. Wang, H. Ma, A. Lv, H. Wang, Q. Wang, M. Gu, S. Cai, Y.; Zhang, L. Fu, M. Zhang, C. Dong, W. Yao, H. Shi, Z. An, W. Huang, *Angew. Chem. Int. Ed.* **2019**, *58*, 14140.
[32] H. Wu, W.; Chi, Z. Chen, G. Liu, L. Gu, A. K. Bindra, G. Yang, X. Liu, Y. Zhao, *Adv. Funct. Mater.* **2019**, *29*, 1807243.
[33] C. Chen, R. Huang, A. S. Batsanov, P. Pander, Y. T. Hsu, Z. Chi, F. B. Dias, M. R. Bryce, *Angew. Chem. Int. Ed*. **2018**, *57*, 16407.
[34] H. Ma, Q. Peng, Z. An, W. Huang, Z. Shuai, *J. Am. Chem. Soc*. **2019**, *141*, 1010.
[35] H. Wu, Y. Zhou, L. Yin, C. Hang, X. Li, H. Ågren, T. Yi, Q. Zhang, L. Zhu, *J. Am. Chem. Soc.* **2017**, *139*, 785.
[36] X. Ma, C. Xu, J. Wang, H. Tian, *Angew. Chem. Int. Ed.* **2018**, *57*, 10854.
[37] S. Cai, H. Ma, H. Shi, H. Wang, X. Wang, L. Xiao, W. Ye, K. Huang, X. Cao, N. Gan, C. Ma, M. Gu, L. Song, H. Xu, Y. Tao, C. Zhang, W. Yao, Z. An, W. Huang, *Nat. Commun.* **2019**, *10*, 4247.
[38] D. Li, F. Lu, J. Wang, W. Hu, X. M. Cao, X. Ma, H. Tian, *J. Am. Chem. Soc.* **2018**, *140*, 1916.
[39] Z. Y. Zhang, Y. Chen, Y. Liu, *Angew. Chem. Int. Ed.* **2019**, *58*, 6028.
[40] T. Watanabe, S. Ueda, S. Inuki, S. Oishi, N. Fujii and H. Ohno, *Chem. Commun.* **2007**, *43*, 4516.
[41] L.-F. Yu, C.-W. Ge, J.-T. Wang, X. Xiang, W.-S. Li, *Polymer* **2015**, *59*, 57.
[42] K. Jankova, X. Chen, J. Kops, W. Batsberg, *Macromolecules* **1998**, *31*, 538.
[43] K. A. Davis, K. Matyjaszewski, *Macromolecules* **2000**, *33*, 4039.
[44] S. N. Sidorov, L. M. Bronstein, Y. A. Kabachii, P. M. Valetsky, P. L. Soo, D. Maysinger, A. Eisenberg, *Langmuir* **2004**, *20*, 3543.
[45] J. Xia, X. Zhang, K. Matyjaszewski, *Macromolecules* **1999**, *32*, 3531.

10.1002/asia.202000965

Entry for the Table of Contents

Insert graphic for Table of Contents here. ((Please ensure your graphic is in **one** of following formats))

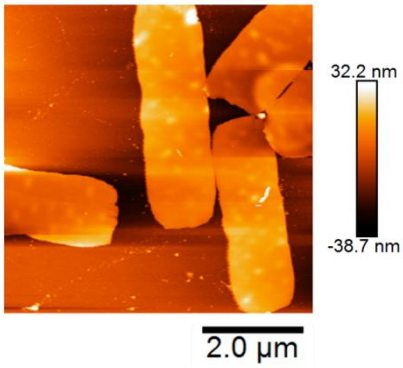

A room-temperature phosphorescence (RTP) system of 9-acetyl-3,6-diiodocarbazole in the crystalline state has been found to show efficient intersystem crossing and pure phosphorescence (fluorescence free) in its steady-state emission spectra. Sheet-like RTP crystalline nanostructures with excellent aqueous dispersity have been obtained by macromolecular self-assembly of 9-acetyl-3,6-diiodocarbazole and amphiphilic triblock copolymers.

Institute and/or researcher Twitter usernames: ((optional))